Supporting Information for

Tetranuclear Dysprosium Single-Molecule Magnets: Tunable Magnetic Interactions and Magnetization Dynamics through Modifying Coordination Number

Kun Zhang,*[,ab] Gao-Peng Li,[b] Vincent Montigaud,[d] Olivier Cador,[d] Boris Le Guennic,*[,d] Jin-Kui Tang*[,c] and Yao-Yu Wang*[,b]

[a] School of Textile Science and Engineering, Xi'an Polytechnic University, Xi'an, 710048, P.R. China.
[b] Key Laboratory of Synthetic and Natural Functional Molecule Chemistry of the Ministry of Education, Shaanxi Key Laboratory of Physico-Inorganic Chemistry, College of Chemistry & Materials Science, Northwest University, Xi'an, 710127, P.R. China.
[c] State Key Laboratory of Rare Earth Resource Utilization, Changchun Institute of Applied Chemistry, Chinese Academy of Sciences, Changchun, 130022, P.R. China.
[d] Univ Rennes, CNRS, ISCR (Institut des Sciences Chimiques de Rennes) - UMR 6226, F-35000 Rennes, France.
E-mail: zhangkun625@foxmail.com; wyaoyu@nwu.edu.cn; tang@ciac.ac.cn; boris.leguennic@univ-rennes1.fr

Supplementary Information Contents

Page	Title
S1	**Table S1.** Crystallographic data for complex **2**. **Figure S1.** Experimental and simulated PXRD patterns of complex **2**.
S2	**Table S2.** Selected bond lengths (Å) and angles (°) for complexes **1** and **2**.
S3	**Table S3.** SHAPE analysis of the Dy(III) ion in complexes **1** and **2**. **Figure S2.** Field dependence of the magnetization, M, at 2, 3 and 5 K for for complex **2** plotted as *M vs. H* and *M vs. H T*$^{-1}$
S4	**Figure S3.** Magnetic hysteresis loops at 1.8 K for complex **2**. **Figure S4.** Comparison of temperature dependent in-phase (χ_M') ac susceptibility for complexes **1** and **2** under zero dc field. **Figure S5.** Frequency dependence in zero dc field of the in-phase (χ') and the out-of-phase (χ'') ac susceptibility component at different temperature for **2**.
S5	**Figure S6.** Cole–Cole plots for **2**. **Table S4.** Relaxation fitting parameters from Least-Squares Fitting of $\chi(f)$ between 1-997 Hz data under zero dc field of complex **2**.
S6	Computational details
S7	**Figure S7.** Thermal variation of the magnetic susceptibility from 2 to 300K for the complex **2** (exp.) and the corresponding computed model **2'**.
S8	**Table S5.** Computed energies levels (the ground state is set at zero), component values of the Lande factor *g* and wavefunction composition for each M_J state of the ground-state multiplet for **Dy1** of the model complex **1'**.
S9	**Table S6.** Computed energies levels (the ground state is set at zero), component values of the Lande factor *g* and wavefunction composition for each M_J state of the ground-state multiplet for **Dy1a** of the model complex **1'**.
S10	**Table S7.** Computed energies levels (the ground state is set at zero), component values of the Lande factor *g* and wavefunction composition for each M_J state of the ground-state multiplet for **Dy2** of the model complex **1'**.
S11	**Table S8.** Computed energies levels (the ground state is set at zero), component values of the Lande factor *g* and wavefunction composition for each M_J state of the ground-state multiplet for **Dy2a** of the model complex **1'**.
S12	**Table S9.** Computed energies levels (the ground state is set at zero), component

	values of the Lande factor *g* and wavefunction composition for each M_J state of the ground-state multiplet for **Dy1** of the model complex **2'**.
S13	**Table S10.** Computed energies levels (the ground state is set at zero), component values of the Lande factor *g* and wavefunction composition for each M_J state of the ground-state multiplet for **Dy1a** of the model complex **2'**.
S14	**Table S11.** Computed energies levels (the ground state is set at zero), component values of the Lande factor *g* and wavefunction composition for each M_J state of the ground-state multiplet for **Dy2** of the model complex **2'**.
S15	**Table S12.** Computed energies levels (the ground state is set at zero), component values of the Lande factor *g* and wavefunction composition for each M_J state of the ground-state multiplet for **Dy2a** of the model complex **2'**.
S16	**References**

Table S1 Crystallographic data for complex **2**.

Complex	**2**[a]
Formula	$C_{62}H_{60}Dy_4N_8O_{22}$
Fw	1919.18
Temp (K)	296(2)
Crystal system	Monoclinic
Space group	$P2_1/n$
a (Å)	16.104(1)
b (Å)	11.332(1)
c (Å)	17.965(2)
α (˚)	90.00
β (˚)	94.292(2)
γ (˚)	90.00
Volume (Å^3)	3269.4(6)
Z	2
D_{calc} (g cm^{-3})	1.950
μ (mm^{-1})	4.602
F (000)	1856
Reflections (all)	6669
Reflections(> 2σ)	4703
R_{int}	0.0404
R_{sigma}	0.0527
R_1, wR_2 ($I > 2\sigma(I)$)	0.0330, 0.0652
R_1, wR_2 (all data)	0.0590, 0.0748
GOF	0.968

[a]See also Li *et al.*[S1]

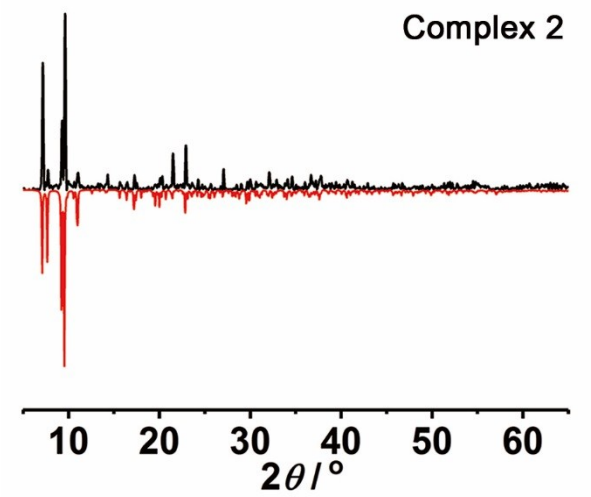

Figure S1. The experimental (black) powder X-ray diffraction and simulated patterns (red) of complex **2**.

Table S2 Selected bond lengths (Å) and angles (°) for complexes **1**[S2] and **2**[S1]

	1	**2**
Dy1-O1	2.362(3)	2.328(3)
Dy1-O1^{a}	2.397(3)	2.347(3)
Dy1-O2	2.339(3)	2.307(3)
Dy1-O3	2.386(3)	2.353(3)
Dy1-O6	2.298(3)	2.293(3)
Dy1-O9	2.565(5)	2.416(5)
Dy1-O10	2.500(3)	2.470(4)
Dy1-O12	2.409(3)	x
Dy1-N1	2.534(3)	2.514(5)
Dy2-O1^{a}	2.353(3)	2.395(3)
Dy2-O2^{a}	2.344(3)	2.383(3)
Dy2-O3	2.346(3)	2.372(3)
Dy2-O4^{a}	2.641(3)	2.539(3)
Dy2-O5	2.203(4)	2.179(4)
Dy2-O6	2.329(3)	2.354(3)
Dy2-O8	2.365(3)	2.373(4)
Dy2-N2	2.464(4)	2.465(5)
Dy1-O1-Dy1^{a}	113.10(10)	109.99(13)
Dy1-O1-Dy2^{a}	110.44(10)	109.58(13)
Dy1^{a}-O1-Dy2^{a}	94.67(9)	93.57(12)
Dy1-O2-Dy2^{a}	111.61(10)	110.74(13)
Dy1-O3-Dy2	95.15(10)	94.02(12)
Dy1-O6-Dy2	98.07(10)	96.10(12)
Dy1⋯Dy2	3.4934(9)	3.4561(6)

Symmetry transformations used to generate equivalent atoms: for **1**, a: 1-x, 1-y, 1-z; for **2**, 1-x,1-y,-z.
Symbol ‘x’ represent that there is no corresponding coordinate atom in complex.

Table S3. SHAPE analysis of the Dy(III) ion in complexes **1**[S2] and **2**[S1]

Label	Shape	Symmetry	Distortion (**1**) Dy1	Label	Shape	Symmetry	Distortion (**2**) Dy1
EP-9	Enneagon	D_{9h}	22.590	OP-8	Octagon	D_{8h}	28.746
OPY-9	Octagonal pyramid	C_{8v}	17.655	HPY-8	Heptagonal pyramid	C_{7v}	20.142
HBPY-9	Heptagonal bipyramid	D_{7h}	19.201	HBPY-8	Hexagonal bipyramid	D_{6h}	18.324
JTC-9	Johnson triangular cupola J3	C_{3v}	12.045	CU-8	Cube	O_h	15.409
JCCU-9	Capped cube J8	C_{4v}	12.784	SAPR-8	Square antiprism	D_{4d}	5.849
CCU-9	Spherical-relaxed capped cube	C_{4v}	12.878	TDD-8	Triangular dodecahedron	D_{2d}	5.213
JCSAPR-9	Capped square antiprism J10	C_{4v}	6.253	JGBF-8	Johnson gyrobifastigium J26	D_{2d}	15.008
CSAPR-9	Spherical capped square antiprism	C_{4v}	6.219	JETBPY-8	Johnson elongated triangular bipyramid J14	D_{3h}	24.759
JTCTPR-9	Tricapped trigonal prism J51	D_{3h}	4.438	JBTPR-8	Biaugmented trigonal prism J50	C_{2v}	6.482
TCTPR-9	Spherical tricapped trigonal prism	D_{3h}	7.202	BTPR-8	Biaugmented trigonal prism	C_{2v}	5.163
JTDIC-9	Tridiminished icosahedron J63	C_{3v}	15.019	JSD-8	Snub diphenoid J84	D_{2d}	7.509
HH-9	Hula-hoop	C_{2v}	12.333	TT-8	Triakis tetrahedron	T_d	15.879
MFF-9	Muffin	C_s	5.779	ETBPY-8	Elongated trigonal bipyramid	D_{3h}	21.507

Label	Shape	Symmetry	Distortion (**1**) Dy2	Distortion (**2**) Dy2
OP-8	Octagon	D_{8h}	29.815	32.596
HPY-8	Heptagonal pyramid	C_{7v}	17.065	19.944
HBPY-8	Hexagonal bipyramid	D_{6h}	17.599	16.790
CU-8	Cube	O_h	11.889	12.346
SAPR-8	Square antiprism	D_{4d}	5.413	6.206
TDD-8	Triangular dodecahedron	D_{2d}	6.459	6.977
JGBF-8	Johnson gyrobifastigium J26	D_{2d}	18.185	16.875
JETBPY-8	Johnson elongated triangular bipyramid J14	D_{3h}	26.187	23.613
JBTPR-8	Biaugmented trigonal prism J50	C_{2v}	5.593	7.170
BTPR-8	Biaugmented trigonal prism	C_{2v}	6.736	7.694
JSD-8	Snub diphenoid J84	D_{2d}	8.145	9.392
TT-8	Triakis tetrahedron	T_d	11.794	12.339
ETBPY-8	Elongated trigonal bipyramid	D_{3h}	24.621	23.798

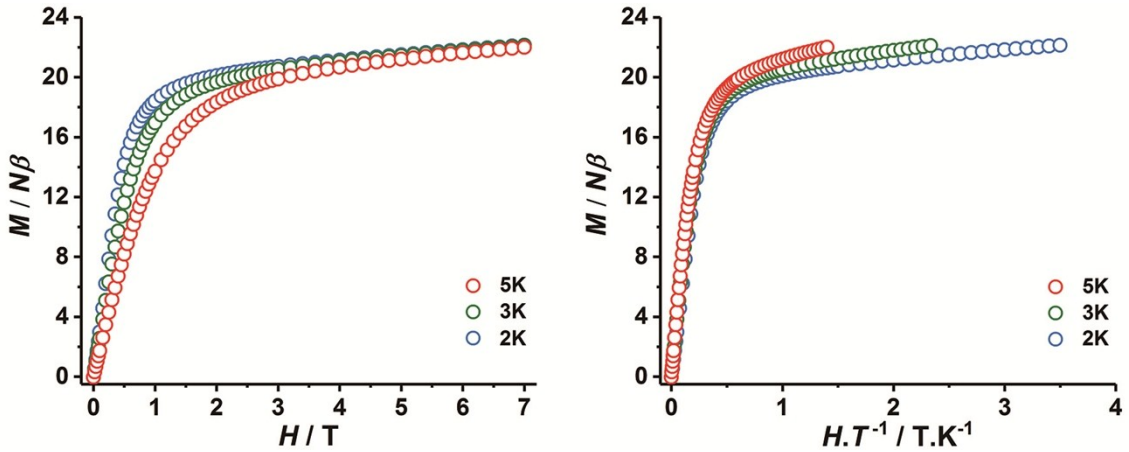

Figure S2. Field dependence of the magnetization, M, at 2, 3 and 5 K for for complex **2** plotted as *M vs. H* (left) and *M vs. H T*$^{-1}$ (right).

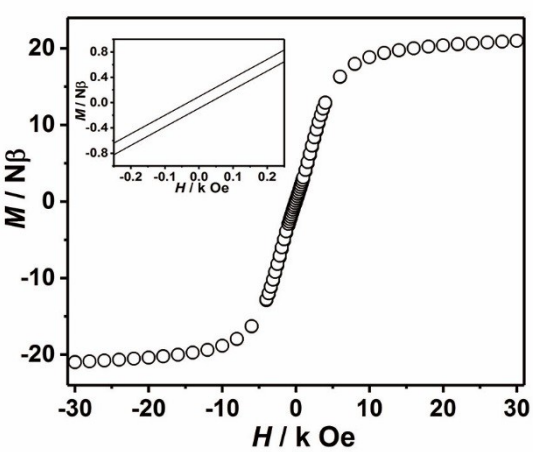

Figure S3. Magnetic hysteresis loops at 1.8 K for complex **2**.

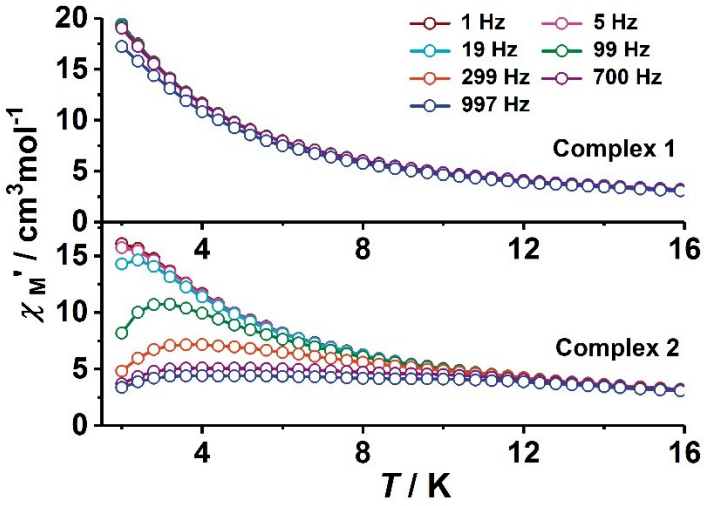

Figure S4. Comparison of temperature dependent in-phase (χ_M') ac susceptibility for complexes **1** and **2** under zero dc field.

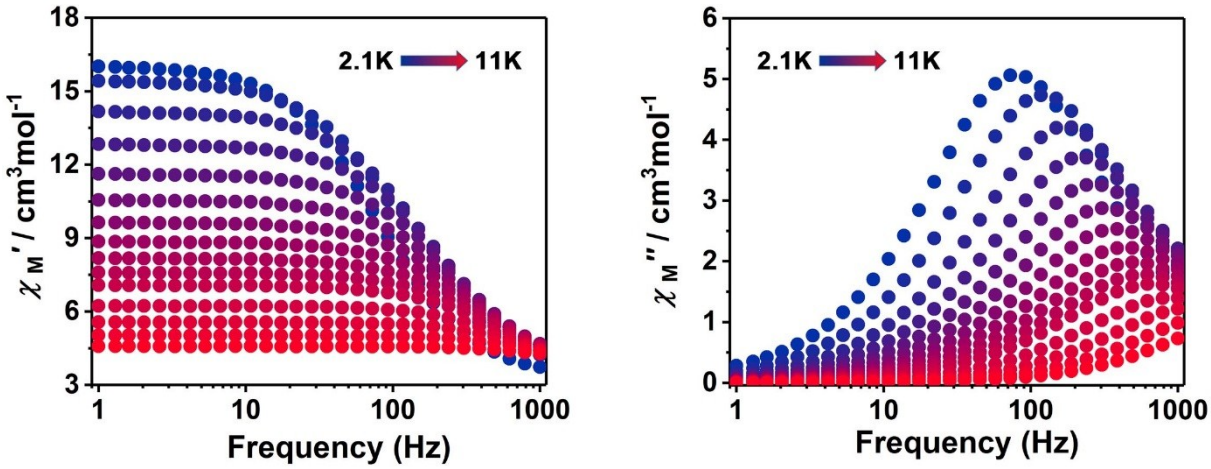

Figure S5. Frequency dependence in zero dc field of the in-phase (χ', left) and the out-of-phase (χ'', right) ac susceptibility component at different temperature for **2**.

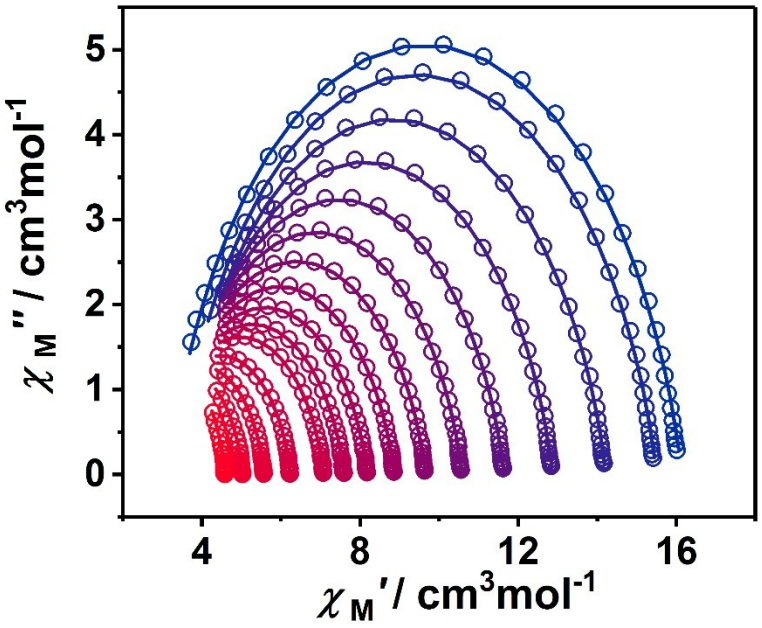

Figure S6. Cole−Cole plots for temperatures between 2.1 and 11 K under a zero dc field with the best fit to the generalized Debye model for **2**. The Solid lines represent fits to the data.

Table S4. Relaxation fitting parameters from Least-Squares Fitting of $\chi(f)$ between 1-997 Hz data under zero dc field of complex **2**.

Temperature	α	τ
2.1K	0.15751	0.00194
2.5K	0.15928	0.0013
3.0K	0.15956	9.16921E-4
3.5K	0.15986	7.13776E-4
4.0K	0.16063	5.86265E-4
4.5K	0.16296	4.93895E-4
5.0K	0.16629	4.19831E-4
5.5K	0.17102	3.58615E-4
6.0K	0.17339	3.09644E-4
6.5K	0.17178	2.70425E-4
7.0K	0.1661	2.35605E-4
8.0K	0.14543	1.74649E-4
9.0K	0.1295	1.16543E-4
10.0K	0.11861	6.90826E-5
11.0K	0.11008	3.457E-5

Computational details:

Wavefunction-based calculations were carried out on a model complex **1'** and **2'** (*vide infra*) by using the SA-CASSCF/RASSI-SO approach as implemented in the MOLCAS *8.0* suite.[S3] In this approach, the relativistic effects are treated in two steps on the basis of the Douglas-Kroll Hamiltonian. First, the scalar terms were included in the basis-set generation and were used to determine the spin-free wavefunctions and energies in the complete active space self-consistent field (CASSCF) method.[S4] Next, spin-orbit coupling was added within the restricted-active-space-state-interaction (RASSI-SO) method, which uses the spin-free wavefunctions as basis states.[S5, S6] The active space of the CASSCF method consisted of the nine electrons spanning the seven *4f* orbitals of the Dy^{3+} ion, i.e. CAS(9,7)SCF. State-Averaged CASSCF calculations were performed for all the sextets (21 roots), all of the quadruplets (224 roots) and 300 out of the 490 doublets. All the sextets, 128 quadruplets and 107 doublets were mixed through spin-orbit coupling in RASSI-SO. The magnetic properties and g-tensors of the lowest states from the energy spectrum were obtained using the pseudo-spin *S = 1/2* formalism in the SINGLE-ANISO routine.[S7, S8] Cholesky decomposition of the bielectronic integrals was employed to save disk space and speed up the calculations.[S9] On the basis of the resulting spin-orbit multiplets the program POLY_ANISO was used to compute the exchange spectrum and the magnetic properties of the complexes.[S10]

The exchange interactions between two anisotropic magnetic centers (Lines model[S11]) are considered in the calculations through the following Hamiltonian:

$$\hat{H}_{ex} = -\sum_{i=1}^{N_c}\sum_{j>i}^{N_c} J_{ij}\tilde{S}_{iz}\tilde{S}_{jz}$$

With $\tilde{S}$ being the pseudospin of the centers i and j, the subscript z denotes the anisotropy axis of the system while J_{ij} represents the effective exchange parameter (fitting parameter) for a given pair ij.

The developped form of the Hamiltonian applied in the case of **2'** is then:

$$\hat{H}_{ex} = -\left(J_{12}\left(\tilde{S}_2\cdot\tilde{S}_1 + \tilde{S}_{1a}\cdot\tilde{S}_{2a}\right) + J_{1a2}\left(\tilde{S}_1\cdot\tilde{S}_{2a} + \tilde{S}_{1a}\cdot\tilde{S}_2\right) + J_{11a}\left(\tilde{S}_1\cdot\tilde{S}_{1a}\right)\right)$$

The calculations have been carried out for each of the four Dy(III) centers with the other three Dy(III) centers replaced by Y(III) ions. All atoms were described by ANO-RCC basis sets. [S12, S13] The following contractions were used: [8s7p4d3f2g1h] for the Dy atom, [6s5p3d1f] for the Y atoms, [3s2p1d] for O and N atoms of the first coordination sphere, [3s2p] for the other N, C and F atoms and [2s] for H atoms. The

atomic positions were extracted from X-ray crystal data. The phenyl groups of the L ligands were truncated and only the atoms from the first coordination sphere were kept and the corresponding truncated C atoms were replaced by H atoms. DFT geometry optimizations of the hydrogen positions were carried out on the Y parent complex with the Gaussian 09 (revision D.01) package[S14] employing the PBE0 hybrid functional.[S15, S16] The "Stuttgart/Dresden" basis sets and effective core potentials were used to describe the yttrium atom,[S17] whereas all other atoms were described with the SVP basis sets.[S18]

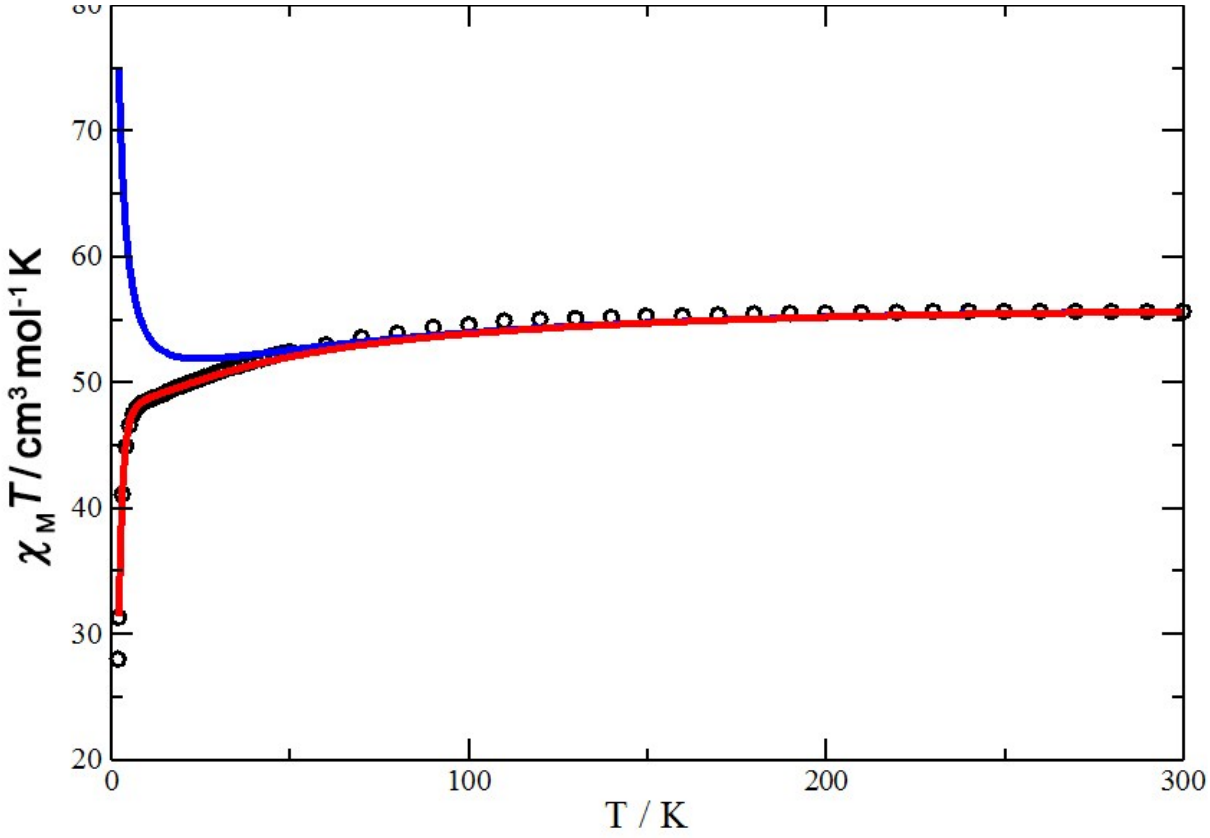

Figure S7. Thermal variation of the magnetic susceptibility from 2 to 300K for the complex **2** (exp.) and the corresponding computed model **2'** (solid lines). The blue curve corresponds to the theoretical model considering only dipolar interactions (J_{dip}) while the red curve corresponds to both dipolar and exchange contributions ($J_{dip} + J_{ex}$).

Table S5. Computed energies levels (the ground state is set at zero), component values of the Lande factor *g* and wavefunction composition for each M_J state of the ground-state multiplet for **Dy1** of model complex **1'**.

KD	Energy (cm^{-1})	g_X	g_Y	g_Z	Wavefunction composition*
1	0.0	0.49	1.22	18.06	0.77 |±15/2> + 0.15 |±11/2>
2	59.9	2.91	5.31	10.42	0.40 |±13/2> + 0.19 |±9/2> + 0.14 |±5/2> + 0.08 |±1/2> + 0.08 |±7/2> + 0.06 |±3/2>
3	107.3	1.65	3.13	7.39	0.36 |±3/2> + 0.15 |±13/2> + 0.13 |±7/2> + 0.11 |±1/2> + 0.09 |±11/2> + 0.07 |±15/2>
4	116.6	2.53	5.44	11.98	0.45 |±1/2> + 0.21 |±5/2> + 0.17 |±3/2> + 0.08 |±13/2>
5	166.9	0.72	1.85	15.09	0.22 |±9/2> + 0.21 |±11/2> + 0.15 |±7/2> + 0.12 |±1/2> + 0.10 |±13/2> + 0.08 |±5/2> + 0.08 |±3/2>
6	224.6	0.70	2.84	12.68	0.29 |±7/2> + 0.25 |±5/2> + 0.14 |±13/2> + 0.10 |±11/2> + 0.08 |±9/2> + 0.07 |±3/2> + 0.05 |±1/2>
7	248.3	0.77	2.52	16.19	0.25 |±3/2> + 0.22 |±5/2> + 0.17 |±1/2> + 0.15 |±7/2> + 0.08 |±11/2> + 0.07 |±9/2> + 0.05 |±13/2>
8	296.6	0.20	0.46	18.49	0.38 |±9/2> + 0.31 |±11/2> + 0.15 |±7/2> + 0.08 |±13/2>

*Only the contributions ≥ 5% are given.

Table S6. Computed energy levels (the ground state is set at zero), component values of the Lande factor *g* and wavefunction composition for each M_J state of the ground-state multiplet for **Dy1a** of model complex **1'**.

KD	Energy (cm^{-1})	g_X	g_Y	g_Z	Wavefunction composition*
1	0.0	0.46	1.10	18.16	0.78 |±15/2> + 0.13 |±11/2>
2	61.5	2.88	5.30	10.67	0.41 |±13/2> + 0.18 |±9/2> + 0.15 |±5/2> + 0.09 |±7/2> + 0.06 |±1/2> + 0.06 |±3/2>
3	109.0	0.14	3.08	7.57	0.35 |±3/2> + 0.16 |±13/2> + 0.11 |±7/2> + 0.11 |±1/2> + 0.09 |±11/2> + 0.07 |±15/2> + 0.05 |±5/2>+ 0.05 |±9/2>
4	120.2	2.04	3.91	13.54	0.52 |±1/2> + 0.19 |±5/2> + 0.17 |±3/2> + 0.06 |±13/2>
5	168.4	0.79	1.93	14.97	0.21 |±11/2> + 0.21 |±9/2> + 0.14 |±7/2> + 0.12 |±1/2> + 0.10 |±13/2> + 0.09 |±5/2> + 0.09 |±3/2>
6	225.5	0.65	2.80	12.69	0.32 |±7/2> + 0.22 |±5/2> + 0.14 |±13/2> + 0.09 |±11/2> + 0.08 |±9/2> + 0.07 |±3/2> + 0.05 |±1/2>
7	249.1	0.78	2.50	16.11	0.25 |±5/2> + 0.24 |±3/2> + 0.15 |±1/2> + 0.14 |±7/2> + 0.08 |±11/2> + 0.07 |±9/2> + 0.06 |±13/2>
8	297.7	0.20	0.46	18.50	0.38 |±9/2> + 0.32 |±11/2> + 0.15 |±7/2> + 0.08 |±13/2>

*Only the contributions ≥ 5% are given.

Table S7. Computed energy levels (the ground state is set at zero), component values of the Lande factor *g* and wavefunction composition for each M_J state of the ground-state multiplet for **Dy2** of model complex **1'**.

KD	Energy (cm^{-1})	g_X	g_Y	g_Z	Wavefunction composition*
1	0.0	0.01	0.01	19.75	0.98 |±15/2> + 0.02 |±11/2>
2	161.3	0.07	0.10	16.98	0.92 |±13/2> + 0.05 |±11/2>
3	307.2	2.50	3.42	12.06	0.68 |±11/2> + 0.10 |±9/2> + 0.07 |±3/2> + 0.05 |±5/2>
4	376.5	1.32	4.15	11.94	0.31 |±1/2> + 0.31 |±9/2> + 0.20 |±3/2> + 0.10 |±5/2>
5	423.6	3.01	4.47	11.85	0.31 |±7/2> + 0.23 |±1/2> + 0.15 |±9/2> + 0.14 |±3/2> + 0.13 |±5/2>
6	521.5	0.90	3.11	12.94	0.26 |±7/2> + 0.23 |±5/2> + 0.18 |±1/2> + 0.16 |±3/2> + 0.09 |±9/2> + 0.06 |±11/2>
7	556.5	0.56	4.16	14.80	0.38 |±5/2> + 0.34 |±3/2> + 0.09 |±9/2> + 0.09 |±7/2> + 0.07 |±1/2>
8	601.2	0.34	0.48	18.49	0.27 |±7/2> + 0.24 |±9/2> + 0.17 |±1/2> + 0.11 |±11/2> + 0.10 |±5/2> + 0.08 |±3/2>

*Only the contributions ≥ 5% are given.

Table S8. Computed energy levels (the ground state is set at zero), component values of the Lande factor *g* and wavefunction composition for each M_J state of the ground-state multiplet for **Dy2a** of model complex **1'**.

KD	Energy (cm^{-1})	g_X	g_Y	g_Z	Wavefunction composition*
1	0.0	0.01	0.01	19.75	0.98 |±15/2> + 0.02 |±11/2>
2	161.7	0.07	0.10	16.98	0.92 |±13/2> + 0.05 |±11/2>
3	308.3	2.51	3.33	12.11	0.68 |±11/2> + 0.10 |±9/2> + 0.07 |±3/2> + 0.05 |±5/2>
4	378.8	1.28	4.02	11.90	0.31 |±1/2> + 0.31 |±9/2> + 0.20 |±3/2> + 0.11 |±5/2>
5	424.3	3.02	4.63	11.67	0.31 |±7/2> + 0.23 |±1/2> + 0.14 |±9/2> + 0.14 |±3/2> + 0.14 |±5/2>
6	522.2	1.03	3.20	12.73	0.26 |±7/2> + 0.22 |±5/2> + 0.19 |±1/2> + 0.16 |±3/2> + 0.10 |±9/2> + 0.06 |±11/2>
7	556.9	0.64	4.36	14.71	0.39 |±5/2> + 0.34 |±3/2> + 0.09 |±9/2> + 0.09 |±7/2> + 0.07 |±1/2>
8	602.6	0.29	0.43	18.56	0.26 |±7/2> + 0.24 |±9/2> + 0.17 |±1/2> + 0.11 |±11/2> + 0.10 |±5/2> + 0.08 |±3/2>

*Only the contributions ≥ 5% are given.

Table S9. Computed energies levels (the ground state is set at zero), component values of the Lande factor *g* and wavefunction composition for each M_J state of the ground-state multiplet for **Dy1** of model complex **2'**.

KD	Energy (cm^{-1})	g_X	g_Y	g_Z	Wavefunction composition*
1	0.0	0.17	0.46	18.45	0.80 |±15/2> + 0.14 |±11/2>
2	61.3	0.83	1.27	15.05	0.33 |±9/2> + 0.33 |±13/2> + 0.17 |±5/2> + 0.06 |±7/2>
3	108.1	1.98	4.96	10.48	0.28 |±13/2> + 0.27 |±7/2> + 0.23 |±3/2> + 0.08 |±1/2> + 0.05 |±15/2>
4	159.3	1.44	5.11	10.80	0.38 |±1/2> + 0.19 |±11/2> + 0.13 |±5/2> + 0.09 |±13/2> + 0.09 |±7/2>
5	203.8	2.16	2.60	14.95	0.27 |±3/2> + 0.26 |±5/2> + 0.15 |±11/2> + 0.11 |±1/2> + 0.07 |±13/2> + 0.07 |±9/2> + 0.06 |±7/2>
6	310.2	0.99	3.85	12.92	0.23 |±1/2> + 0.22 |±11/2> + 0.21 |±3/2> + 0.10 |±9/2> + 0.07 |±13/2> + 0.07 |±7/2> + 0.07 |±5/2>
7	333.7	0.92	4.41	14.04	0.27 |±9/2> + 0.21 |±7/2> + 0.16 |±5/2> + 0.10 |±13/2> + 0.09 |±11/2> + 0.07 |±1/2> + 0.07 |±3/2>
8	452.0	0.00	0.01	19.03	0.22 |±7/2> + 0.19 |±9/2> + 0.17 |±5/2> + 0.13 |±11/2> + 0.12 |±3/2> + 0.09 |±1/2> + 0.07 |±13/2>

* : Only the contributions ≥ 5% are given.

Table S10. Computed energies levels (the ground state is set at zero), component values of the Lande factor *g* and wavefunction composition for each M_J state of the ground-state multiplet for **Dy1a** of model complex **2'**.

KD	Energy (cm^{-1})	g_X	g_Y	g_Z	Wavefunction composition*
1	0.0	0.17	0.46	18.45	0.80 |±15/2> + 0.14 |±11/2>
2	61.3	0.83	1.27	15.05	0.33 |±9/2> + 0.33 |±13/2> + 0.17 |±5/2> + 0.06 |±7/2>
3	108.1	1.98	4.96	10.48	0.28 |±13/2> + 0.27 |±7/2> + 0.23 |±3/2> + 0.08 |±1/2> + 0.05 |±15/2>
4	159.3	1.44	5.11	10.80	0.38 |±1/2> + 0.19 |±11/2> + 0.13 |±5/2> + 0.09 |±13/2> + 0.09 |±7/2> + 0.06 |±3/2> + 0.05 |±15/2>
5	203.8	2.16	2.60	14.95	0.27 |±3/2> + 0.26 |±5/2> + 0.15 |±11/2> + 0.11 |±1/2> + 0.07 |±13/2> + 0.07 |±9/2> + 0.06 |±7/2>
6	310.2	0.99	3.85	12.92	0.23 |±1/2> + 0.22 |±11/2> + 0.21 |±3/2> + 0.10 |±9/2> + 0.07 |±13/2> + 0.07 |±7/2> + 0.07 |±5/2>
7	333.7	0.92	4.41	14.05	0.27 |±9/2> + 0.21 |±7/2> + 0.16 |±5/2> + 0.10 |±13/2> + 0.09 |±11/2> + 0.07 |±1/2> + 0.07 |±3/2>
8	452.0	0.00	0.01	19.03	0.22 |±7/2> + 0.19 |±9/2> + 0.17 |±5/2> + 0.13 |±11/2> + 0.12 |±3/2> + 0.09 |±1/2> + 0.07 |±13/2>

* : Only the contributions ≥ 5% are given.

Table S11. Computed energies levels (the ground state is set at zero), component values of the Lande factor *g* and wavefunction composition for each M_J state of the ground-state multiplet for **Dy2** of model complex **2'**.

KD	Energy (cm^{-1})	g_X	g_Y	g_Z	Wavefunction composition*
1	0.0	0.01	0.02	19.67	0.97 |±15/2>
2	152.5	0.31	0.44	16.66	0.88 |±13/2> + 0.05 |±11/2>
3	263.4	3.00	4.08	11.66	0.50 |±11/2> + 0.13 |±5/2> + 0.11 |±3/2> + 0.09 |±9/2> + 0.07 |±1/2> + 0.06 |±7/2>
4	324.2	1.76	4.85	8.44	0.26 |±9/2> + 0.24 |±3/2> + 0.20 |±1/2> + 0.19 |±11/2> + 0.07 |±5/2>
5	378.2	4.08	5.73	10.18	0.32 |±1/2> + 0.29 |±7/2> + 0.22 |±9/2> + 0.09 |±5/2> + 0.06 |±3/2>
6	465.4	0.78	2.31	13.14	0.36 |±7/2> + 0.29 |±5/2> + 0.14 |±3/2> + 0.08 |±1/2> + 0.05 |±9/2>
7	492.7	0.27	3.47	13.35	0.32 |±3/2> + 0.32 |±5/2> + 0.15 |±9/2> + 0.11 |±11/2>
8	513.3	1.01	1.40	16.23	0.28 |±1/2> + 0.20 |±9/2> + 0.20 |±7/2> + 0.13 |±3/2> + 0.09 |±11/2> + 0.08 |±5/2>

* : Only the contributions ≥ 5% are given.

Table S12. Computed energies levels (the ground state is set at zero), component values of the Lande factor *g* and wavefunction composition for each M_J state of the ground-state multiplet for **Dy2a** of model complex **2'**.

KD	Energy (cm^{-1})	g_X	g_Y	g_Z	Wavefunction composition*
1	0.0	0.01	0.02	19.67	0.97 |±15/2>
2	152.5	0.31	0.44	16.66	0.88 |±13/2> + 0.05 |±11/2>
3	263.4	3.00	4.08	11.66	0.50 |±11/2> + 0.13 |±5/2> + 0.11 |±3/2> + 0.09 |±9/2> + 0.07 |±1/2> + 0.06 |±7/2>
4	324.2	1.77	4.85	8.44	0.26 |±9/2> + 0.24 |±3/2> + 0.20 |±1/2> + 0.19 |±11/2> + 0.07 |±5/2>
5	378.1	4.08	5.73	10.18	0.32 |±1/2> + 0.29 |±7/2> + 0.22 |±9/2> + 0.09 |±5/2> + 0.06 |±3/2>
6	465.3	0.78	2.31	13.14	0.36 |±7/2> + 0.29 |±5/2> + 0.14 |±3/2> + 0.08 |±1/2> + 0.05 |±9/2>
7	492.7	0.27	3.47	13.35	0.32 |±3/2> + 0.32 |±5/2> + 0.14 |±9/2> + 0.11 |±11/2> + 0.04 |±1/2>
8	513.3	1.01	1.40	16.23	0.28 |±1/2> + 0.20 |±9/2> + 0.20 |±7/2> + 0.13 |±3/2> + 0.09 |±11/2> + 0.08 |±5/2>

* : Only the contributions ≥ 5% are given.

References

[S1] Zhang, H. F.; Zhang, J.; Li, Y. H.; Qin, Y. R.; Chen, Y. M.; Liu, W.; Gao, D. D.; Li, W. *J. Coord. Chem.* **2015**, *68*, 2798−2809.

[S2] Zhang, K.; Montigaud, V.; Cador, O.; Li, G. P.; Le Guennic, B.; Tang, J.; Wang, Y.-Y. Tuning the Magnetic Interactions in $Dy(III)_4$ Single-Molecule Magnets. *Inorg. Chem.* **2018**, *57*, 8550−8557.

[S3] Aquilante, F.; Autschbach, J.; Carlson, R. K.; Chibotaru, L. F.; Delcey, M. G.; De Vico, L.; Galván, I. F.; Ferré, N.; Frutos, L. M.; Gagliardi, L.; Garavelli, M.; Giussani, A.; Hoyer, C. E.; Manni, G. L.; Lischka, H.; Ma, D. X.; Malmqvist, P.; Müller, T.; Nenov, A.; Olivucci, M.; Pedersen, T. B.; Peng, D. L. ; Plasser, F.; Pritchard, B.; Reiher, M. ; Rivalta, I.; Schapiro, I.; Segarra-Martí, J.; Stenrup, M.; Truhlar, D. G. ; Ungur, L.; Valentini, A.; Vancoillie, S.; Veryazov, V.; Vysotskiy, V. P.; Weingart, O.; Zapata, F.; Lindh, R. Molcas 8: New Capabilities for Multiconfigurational Quantum Chemical Calculations Across the Periodic Table. *J. Comput. Chem*. **2016**, *37*, 506−541.

[S4] Roos, B. O.; Taylor, P. R.; Siegbahn, P. E. M. A Complete Active Space SCF Method (CASSCF) Using a Density Matrix Formulated Super-CI Approach. *Chem. Phys.* **1980**, *48*, 157–173.

[S5] Malmqvist, P.Å.; Roos, B.O.; Schimmelpfennig, B. The Restricted Active Space (RAS) State Interaction Approach with Spin-Orbit Coupling. *Chem. Phys. Lett.* **2002**, *357*, 230–240.

[S6] Malmqvist, P.-Å.; Roos, B.O. The CASSCF State Interaction Method. *Chem. Phys. Lett.* **1989**, *155*, 189–194.

[S7] Chibotaru, L.F.; Ungur, L. *Ab Initio* Calculation of Anisotropic Magnetic Properties of Complexes. I. Unique Definition of Pseudospin Hamiltonians and Their Derivation. *J. Chem. Phys.* **2012**, *137*, 064112.

[S8] Chibotaru, L.; Ungur, L.; Soncini, A. The Origin of Nonmagnetic Kramers Doublets in the Ground State of Dysprosium Triangles: Evidence for a Toroidal Magnetic Moment. *Angew. Chem., Int. Ed.* **2008**, *47*, 4126–4129.

[S9] Aquilante, F.; Malmqvist, P.-Å.; Pedersen, T.B.; Ghosh, A.; Roos, B.O. Cholesky Decomposition-Based Multiconfiguration Second-Order Perturbation Theory (CD-CASPT2): Application to the Spin-State Energetics of Co^{III}(diiminato)(NPh). *J. Chem. Theory Comput.* **2008**, *4*, 694–702.

[S10] Chibotaru, L. F.; Ungur, L. The Computer Programs SINGLE_ANISO and POLY_ANISO. **2006**, University of Leuven.

[S11] Lines, M. E. Orbital Angular Momentum in the Theory of Paramagnetic Clusters. *J. Chem. Phys.*, **1971**, *55*, 2977.

[S12] Roos, B. O.; Lindh, R.; Malmqvist, P. A.; Veryazov, V.; Widmark, P. O. Main Group Atoms and Dimers Studied with A New Relativistic ANO Basis Set. *J. Phys. Chem. A.* **2004**, *108*, 2851–2858.

[S13] Roos, B. O.; Lindh, R.; Malmqvist, P.; Veryazov, V.; Widmark, P. O.; Borin, A. C. New Relativistic Atomic Natural Orbital Basis Sets for Lanthanide Atoms with Applications to the Ce Diatom and LuF_3. *J. Phys. Chem. A.* **2008**, *112*, 11431−11435.

[S14] Frisch, M. J.; Trucks, G. W.; Schlegel, H. B.; Scuseria, G. E.; Robb, M. A.; Cheeseman, J. R.; Scalmani, G.; Barone, V.; Mennucci, B.; Petersson, G. A.; Nakatsuji, H.; Caricato, M.; Li, X.; Hratchian, H. P.; Izmaylov, A. F.; Bloino, J.; Zheng, G.; Sonnenberg, J. L.; Hada, M.; Ehara, M.; Toyota, K.; Fukuda, R.; Hasegawa, J.; Ishida, M.; Nakajima, T.; Honda, Y.; Kitao, O.; Nakai, H.; Vreven, T.; Montgomery, J.

A. Jr.; Peralta, J. E.; Ogliaro, F.; Bearpark, M.; Heyd, J. J.; Brothers, E.; Kudin, K. N.; Staroverov, V. N.; Kobayashi, R.; Normand, J.; Raghavachari, K.; Rendell, A.; Burant, J. C.; Iyengar, S. S.; Tomasi, J.; Cossi, M.; Rega, N.; Millam, N. J.; Klene, M.; Knox, J. E.; Cross, J. B.; Bakken, V.; Adamo, C.; Jaramillo, J.; Gomperts, R.; Stratmann, R. E.; Yazyev, O.; Austin, A. J.; Cammi, R.; Pomelli, C.; Ochterski, J. W.; Martin, R. L.; Morokuma, K.; Zakrzewski, V. G.; Voth, G. A.; Salvador, P.; Dannenberg, J. J.; Dapprich, S.; Daniels, A. D.; Farkas, Ö.; Foresman, J. B.; Ortiz, J. V.; Cioslowski, J.; Fox, D. J. *Gaussian 09 Revision D.01*; Gaussian Inc.: Wallingford, CT, USA, **2013**.

[S15] Perdew, J. P.; Burke, K.; Ernzerhof, M. Generalized Gradient Approximation Made Simple. *Phys. Rev. Lett.* **1996**, *77*, 3865–3868.

[S16] Adamo, C.; Barone, V. Toward Reliable Density Functional Methods without Adjustable Parameters: The PBE0 Model. *J. Chem. Phys.* **1999**, *110*, 6158–6170.

[S17] Dolg, M.; Stoll, H.; Preuss, H. A Combination of Quasirelativistic Pseudopotential and Ligand Field Calculations for Lanthanoid Compounds. *Theor. Chim. Acta.* **1993**, *85*, 441–450.

[S18] Weigend, F.; Ahlrichs, R. Balanced Basis Sets of Split Valence, Triple Zeta Valence and Quadruple Zeta Valence Quality for H to Rn: Design and Assessment of Accuracy. *Phys. Chem. Chem. Phys.* **2005**, *7*, 3297–3305.